MOX-Report No. 23/2018

A seamless extension of DG methods for hyperbolic problems to unbounded domains

Benacchio, T.;Bonaventura,L.

MOX, Dipartimento di Matematica
Politecnico di Milano, Via Bonardi 9 - 20133 Milano (Italy)

mox-dmat@polimi.it http://mox.polimi.it

A seamless extension of DG methods for hyperbolic problems to unbounded domains

Tommaso Benacchio [(1)], Luca Bonaventura [(2)]

March 29, 2018

[(1)] Met Office
Exeter
United Kingdom
tommaso.benacchio@metoffice.gov.uk

[(2)] MOX – Modelling and Scientific Computing,
Dipartimento di Matematica, Politecnico di Milano
Via Bonardi 9, 20133 Milano, Italy
luca.bonaventura@polimi.it

Keywords: Laguerre functions; spectral methods; discontinuous Galerkin methods; open boundary conditions; domain decomposition; hyperbolic equations.

AMS Subject Classification: 65M60, 65M70, 65Z99, 76M10, 76M22.

Abstract

We consider spectral discretizations of hyperbolic problems on unbounded domains using Laguerre basis functions. Taking as model problem the scalar advection equation, we perform a comprehensive stability analysis that includes strong collocation formulations, nodal and modal weak formulations, with either inflow or outflow boundary conditions, using either Gauss - Laguerre or Gauss - Laguerre - Radau quadrature nodes and based on either scaled Laguerre functions or scaled Laguerre polynomials. We show that some of these combinations give rise to intrinsically unstable schemes, while the combination of scaled Laguerre functions with Gauss - Laguerre - Radau nodes appears to be stable for both strong and weak formulations. We then show how a modal discretization approach for hyperbolic systems on an unbounded domain can be naturally and seamlessly coupled to a discontinuous finite element discretization on a finite domain. Examples of one dimensional hyperbolic systems are solved with the proposed domain decomposition technique. The errors obtained with the proposed approach are found to be small, enabling the use of the coupled scheme for the simulation of Rayleigh damping layers in the semi-infinite part. Energy errors and reflection ratios of the scheme in absorbing wavetrains and single Gaussian signals show that a small number of nodes in the semi-infinite domain are sufficient to damp the waves. The theoretical insight and numerical results corroborate previous findings by the authors and establish the scaled Laguerre functions-based discretization as a flexible and efficient tool for absorbing layers as well as for the accurate simulation of waves in unbounded regions.

1 Introduction

Accurate numerical solution of wave propagation problems in unbounded domains remains to the present day an unsolved challenge. Practical applications of great importance include modelling of the upper terrestrial atmosphere and of the solar corona, space weather simulations and propagation of electromagnetic waves from a localized source into the far field. In other contexts such as numerical weather prediction, for computational reasons the domain of the hyperbolic differential problem is restricted to a bounded region of interest, the size of which depends on the phenomena under consideration. Boundary conditions are then imposed to the new domain such that outgoing waves can propagate from the bounded domain without spurious reflections. The issue of how to set these open boundary conditions in an analytically consistent and numerically accurate and efficient way has been the object of research for the past four decades [18, 31, 34].

On the one hand, analytical approaches have aimed at imposing radiation or characteristic boundary conditions modelling outgoing disturbances as solutions of reduced model dynamics, see [15, 22] as well as [10, 11, 29] more specifically on environmental fluid dynamics. On the other hand, tackling the problem numerically requires the placement of a buffer region next to the artificial boundary where the outgoing disturbances are relaxed towards a prescribed external solution, commonly the absence of perturbations, that in turn calls for the addition of a diffusive or reactive term in the buffer region [14, 23, 24, 25]. Especially challenging in the setup of these absorbing layers is the choice of resolution, as finer grid spacings enable a better absorption of the outgoing waves, yet incur a higher computational cost. Advanced perfectly matched layer formulations, popular in electro- and elastodynamics as well as computational aeroacoustics, aim at matching analytical formulations on either side of the interface between the bounded and unbounded region, while optimally tuning relaxation parameters in the layer [1, 7, 19, 27, 28, 30, 37]. Despite the substantial efforts in this context, the choice of parameters such as layer thickness and relaxation coefficients is still largely driven by bespoke criteria [26]. Yet another approach is given by infinite elements, whose shape functions mimick the asymptotic behaviour of the solution at infinity [3, 16]. Use of infinite elements-based methodologies does not require splitting the original unbounded domain, yet it entails mapping and modulation by decay functions.

In most cases, both the coupling conditions and the damping

setup often rest on restrictive assumptions on the form of outgoing waves [2]. However, approaches demanding an *ad hoc* identification of waves appear ill-suited to the manifold nature of wavelike solutions impinging on the artificial ceiling of the computational domain in environmental fluid dynamics problems [13]. Furthermore, as more computational power becomes available, modellers are faced with the complementary requirements of simulating ever larger portions of unbounded domains while achieving efficient control over spurious reflections at the upper boundary [17, 20]. As a point of reference, numerical models for operational weather forecasting and climate research routinely devote up to a quarter of the computational power in their simulations to eliminate unwanted perturbations in the upper atmosphere regions. This cost is bound to increase in future high-resolution models as the size needed for the absorbing layer increases with increasing horizontal grid-spacing.

In order to overcome the drawbacks of currently employed approaches, in [5, 6] the authors devised the first application of scaled Laguerre function discretizations to wave propagation problems, using a spectral collocation method for the shallow water equations on the positive half line. By tuning the scaling parameter, the set of quadrature nodes associated with the basis spans a differently-sized portion of the unbounded domain [32, 33, 36, 38]. As shown in [6], this approach to unbounded domains could be coupled to standard discretizations on finite size domains, in order to achieve a convenient framework for effective and economical implementation of open boundary conditions. The strategy entailed a significant reduction in the computational cost of an absorbing layer.

In the present work, we first assess the many possible variants for a discretization of hyperbolic wave propagation problems on unbounded domains using Laguerre basis functions. Choosing the linear advection equation on the domain $\mathbb{R}^+ = [0, +\infty)$ as model problem, we find that discretizations based on scaled Laguerre functions, rather than scaled Laguerre polynomials, and Gauss-Laguerre-Radau quadrature nodes, rather than Gauss-Laguerre nodes, yield stable spectra for the semidiscrete problem in space.

We then extend the framework of [6] and couple a Laguerre spectral discretization to a finite element discretization. More specifically, the domain is split into a bounded interval of size L, where the system is discretized with a standard Discontinuous Galerkin (DG) approach, and a complementary unbounded interval, where the chosen Laguerre spectral approach is employed, so that $\mathbb{R}^+ = [0, L] \cup [L, +\infty)$. We focus here on DG discretization approaches, since the discontinuous nature of the basis functions allows for eas-

ier coupling to the discretization on the semi-infinite domain. We show that a modal Laguerre spectral element scheme can be coupled seamlessly to a modal DG discretization on the finite domain, providing a convenient framework to extend finite domain discretizations and to implement open boundary conditions efficiently via absorbing layers. Numerical experiments are then performed, repeating some of the tests already presented in [6], showing that the accuracy of the proposed approach and its efficiency in implementing absorbing layers improve those of our previous work.

The structure of the paper is as follows. The spectral stability analysis of Laguerre discretizations of scalar advection is discussed in Section 2. The case of hyperbolic systems is tackled in Section 3, while in Section 4 an outline of the coupling strategy is presented. Section 5 contains the numerical results and Section 6 some conclusions and discussion of future work.

2 Stability analysis of scaled Laguerre discretizations of the advection equation

We plan to analyze different discretizations of hyperbolic equations on semi-infinite domains, in order to understand which approach is most convenient to couple with finite element discretizations on finite domains. For this purpose, we start considering the advection equation as a prototype of hyperbolic problems. In strong form, the advection equation is given by

$$\frac{\partial q}{\partial t} + u\frac{\partial q}{\partial z} = 0 \qquad z \in \mathbb{R}^+ = [0, +\infty). \tag{1}$$

This equation should be complemented by the condition

$$\lim_{z \to +\infty} q(z,t) = 0$$

and by Dirichlet boundary condition $q(0,t) = q_L$ when $u > 0$, while in the case $u < 0$ no boundary conditions should be assigned, nor required by the discretization method. It is also assumed that

To derive the corresponding weak form, we integrate equation (1) against a test function φ to obtain

$$\frac{d}{dt}\int_0^{+\infty} \varphi(z) q(z,t)\omega(z)\, dz + u\int_0^{+\infty} \varphi(z)\frac{\partial q}{\partial z}(z,t)\omega(z)\, dz = 0 \tag{2}$$

If scaled Laguerre functions are used, $\omega = 1$. We can then integrate by parts and obtain, in the inflow case,

$$\frac{d}{dt}\int_0^{+\infty} \varphi(z)q(z,t)\,dz - uq_L\varphi(0) - u\int_0^{+\infty} \varphi'(z)q(z,t)\,dz = 0. \quad (3)$$

In the outflow case, in order to have a well posed problem, the solution should not be prescribed at the boundary, so that one should write instead

$$\frac{d}{dt}\int_0^{+\infty} \varphi(z)q(z,t)\,dz - uq(0,t)\varphi(0) - u\int_0^{+\infty} \varphi'(z)q(z,t)\,dz = 0. \quad (4)$$

In case we want to use scaled Laguerre polynomials as basis and test functions, we have to assume instead $\omega(z) = \exp(-\beta z)$ in (2) before integrating by parts. Since

$$\varphi\frac{\partial q}{\partial z}\omega = \frac{\partial}{\partial z}(\varphi q\omega) - \varphi q\frac{\partial \omega}{\partial z} - \frac{\partial \varphi}{\partial z}q\omega = \frac{\partial}{\partial z}(\varphi q\omega) + \beta\varphi q\omega - \frac{\partial \varphi}{\partial z}q\omega, \quad (5)$$

where we have used the fact that $\frac{\partial \omega}{\partial z} = -\beta\omega$, we can obtain, in the inflow case,

$$\frac{d}{dt}\int_0^{+\infty} \varphi(z)q(z,t)\omega(z)\,dz + \beta u\int_0^{+\infty} \varphi(z)q(z,t)\omega(z)\,dz - uq_L\varphi(0)\omega(0) - u\int_0^{+\infty} \varphi'(z)q(z,t)\omega(z)\,dz = 0 \quad (6)$$

and in the outflow case

$$\frac{d}{dt}\int_0^{+\infty} \varphi(z)q(z,t)\omega(z)\,dz + \beta u\int_0^{+\infty} \varphi(z)q(z,t)\omega(z)\,dz - uq(0,t)\varphi(0)\omega(0) - u\int_0^{+\infty} \varphi'(z)q(z,t)\omega(z)\,dz = 0. \quad (7)$$

Several alternatives are then possible for the numerical discretization. As test and basis functions, one may choose a) scaled Laguerre functions or b) scaled Laguerre polynomials. Option a) has the advantage of avoiding the presence of a weight in the scalar product, while option b) has the advantage of allowing to approximate constant functions on $\mathbb{R}^+$. Equation (1) can then be discretized 1) in strong form by a collocation approach using Gauss-Laguerre Radau (GLR) nodes, which is the only practical alternative if Dirichlet b.c. have to be imposed, 2) in weak form, using either GLR or Gauss Laguerre (GL) nodes for numerical integration. Furthermore for option 2), either a nodal discretization (2n) can be used, in which the

basis functions considered are Lagrange basis functions associated with the chosen integration nodes, or a modal discretization (2m). In all cases, spatial discretization results in an ODE system

$$\frac{d\mathbf{q}}{dt} = \mathbf{A}\mathbf{q} + \mathbf{g}, \tag{8}$$

where $\mathbf{q}$ denotes the vector of the degrees of freedom of the spatially discretized problem, $\mathbf{A}$ the discretization of the advection operator and $\mathbf{g}$ is a source term that depends on the Dirichlet b.c. in the inflow boundary $u > 0$ case, while $\mathbf{g} = \mathbf{0}$ in the outflow boundary $u < 0$ case.

We want to study the eigenvalue structure of $\mathbf{A}$ in order to better understand possible stability and accuracy issues in the coupling to discretizations on finite domains. We adopt mostly the notation of [5], [6] and denote by β a scaling parameter, by z_l^β, $l = 0, \ldots, M$ the scaled GLR (SGLR) or the scaled GL (SGL) nodes. We denote by ω_l^β the associated weights and $\hat{h}_l^\beta$ are the associated Lagrange interpolation functions.

Strong form, collocation approach with SGLR nodes and scaled Laguerre functions

We first consider the case a1 (strong collocation form with SGLR nodes and scaled Laguerre functions). We consider the outflow and inflow cases separately. For the inflow case,

$$q_i' = -uq_L(\hat{h}_0^\beta)'(z_i^\beta) - u\sum_{j=1}^{M} q_j(\hat{h}_j^\beta)'(z_i^\beta) \qquad i = 1, \ldots, M. \tag{9}$$

In the outflow case, one has instead

$$q_i' = -u\sum_{j=0}^{M} q_j(\hat{h}_j^\beta)'(z_i^\beta) \qquad i = 0, \ldots, M. \tag{10}$$

In matrix notation, equation (9) yields in the inflow case an ODE system like equation (8) with $\mathbf{q} = [q_1, \ldots, q_M]^T$,

$$\mathbf{A} = -u(\mathbf{D}_\beta)_M, \qquad \mathbf{g} = -uq_L\left[(\hat{h}_0^\beta)'(z_1^\beta), \ldots, (\hat{h}_0^\beta)'(z_M^\beta)\right]^T \tag{11}$$

where, in the notation of [6], $\mathbf{D}_\beta$ denotes the SLGR differentiation matrix and $(\mathbf{D}_\beta)_M$ denotes the $M \times M$ matrix obtained selecting the last M rows and columns of $\mathbf{D}_\beta$. For the outflow case, $\mathbf{q} =$

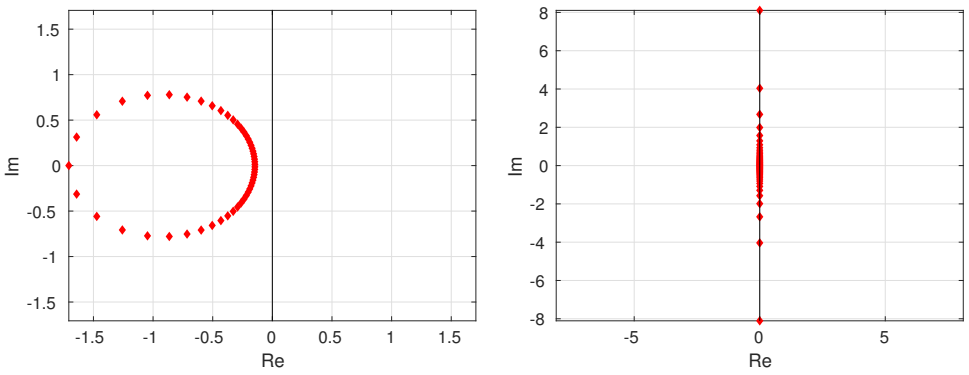

(a) (b)

Figure 1: Eigenvalues in the a1 case, for parameter values $\beta = 1$, $M = 50$ in the a) outflow case $u = -1$ and b) inflow case $u = 1$.

$[q_0, \ldots, q_M]^T$, $\mathbf{g} = \mathbf{0}$ and $\mathbf{A} = -u\mathbf{D}_\beta$. Examples of eigenvalue plots for $\mathbf{A}$ in the a1 case are shown in Figure 1. It can be seen that no stability problems arise, since the real part of all eigenvalues are non positive.

Strong form, collocation approach with SGLR nodes and scaled Laguerre polynomials

If scaled Laguerre polynomials instead of Laguerre functions are used (see [32, 33] for definitions), one gets the discretized equations (9) and (10) with, instead of $\hat{h}_j^\beta$, the Lagrange interpolation functions h_j^β associated with the nodes and weights obtained considering the scaled Laguerre polynomials basis, and $\mathbf{D}_\beta$ now denoting the SGLR differentiation matrix relative to that basis. Examples of eigenvalue plots for $\mathbf{A}$ in this case are shown in figure 2. It can be seen that the inflow case does not display any stability issue, while in the outflow case matrix has some eigenvalues with positive real part.

Weak form, nodal approach with scaled Laguerre functions

For the case of weak form, nodal discretizations based on scaled Laguerre functions, we take again as test and basis functions the Lagrange interpolation functions associated with the SGL or SGLR

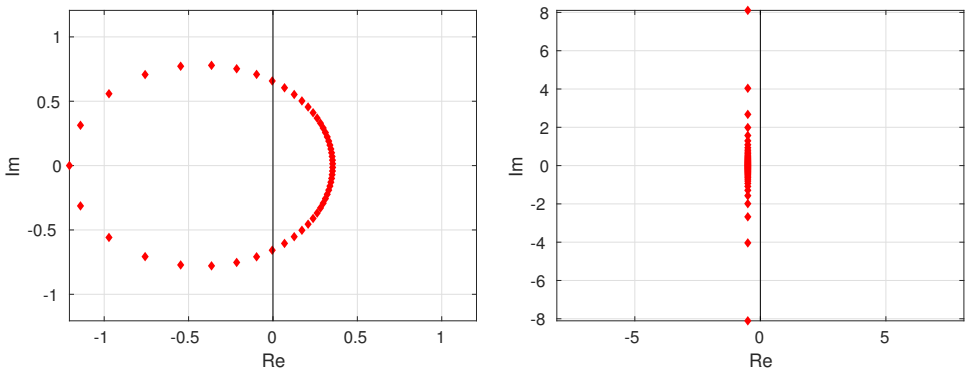

(a) (b)

Figure 2: Eigenvalues in the a1 case, scaled Laguerre polynomials, for parameter values $\beta = 1$, $M = 50$ in the a) outflow case $u = -1$ and b) inflow case $u = 1$.

nodes. We then use the fact that

$$q(z) \approx \sum_{j=0}^{M} q_j \hat{h}_j^\beta(z). \tag{12}$$

We consider the SGL nodes first. Using the fact that the basis functions are also a Lagrange basis and employing the corresponding numerical integration rule, in the inflow case we get from (3)

$$q_i' \omega_i^\beta = u q_L \hat{h}_i^\beta(0) + u \sum_{j=0}^{M} q_j (\hat{h}_j^\beta)'(z_i^\beta) \omega_j^\beta \quad i = 0, \ldots, M \tag{13}$$

and in the outflow case from (4)

$$q_i' \omega_i^\beta = u \sum_{j=0}^{M} q_j \hat{h}_j^\beta(0) \hat{h}_i^\beta(0) + u \sum_{j=0}^{M} q_j (\hat{h}_j^\beta)'(z_i^\beta) \omega_j^\beta \quad i = 0, \ldots, M. \tag{14}$$

In matrix notation, equation (13) yields in the inflow case an ODE system like equation (8) with

$$\mathbf{A} = u \mathbf{\Omega}^{-1} \mathbf{D}_\beta \mathbf{\Omega}, \tag{15}$$

where $\mathbf{\Omega}$ is the diagonal matrix with the weights on the main diagonal, and

$$\mathbf{g} = u q_L \mathbf{\Omega}^{-1} \mathbf{h}, \tag{16}$$

where we have set $\mathbf{h} = [\hat{h}_0^\beta(0), \ldots, \hat{h}_M^\beta(0)]^T$. For the outflow case, equation (14) yields instead $\mathbf{g} = \mathbf{0}$ and

$$\mathbf{A} = u \mathbf{\Omega}^{-1} \mathbf{H} + u \mathbf{\Omega}^{-1} \mathbf{D}_\beta \mathbf{\Omega}, \tag{17}$$

where $\mathbf{H} = \mathbf{h}\mathbf{h}^T$.

For the case of SGLR nodes, one has in the inflow case,

$$q_i'\omega_i^\beta = uq_L(\hat{h}_0^\beta)'(z_i^\beta)\omega_0^\beta + u\sum_{j=1}^{M} q_j(\hat{h}_j^\beta)'(z_i^\beta)\omega_j^\beta \quad i = 1,\ldots,M. \quad (18)$$

where we have used the fact that for the SGLR Lagrangian basis one has $\hat{h}_i^\beta(0) = 0$ for $i = 1,\ldots,M$ while $\hat{h}_0^\beta(0) = 1$. In the outflow case, one has instead

$$q_i'\omega_i^\beta = u\sum_{j=0}^{M} q_j(\hat{h}_j^\beta)'(z_i^\beta)\omega_j^\beta, \quad i = 1,\ldots,M \quad (19)$$

while for $i = 0$ one obtains:

$$q_0'\omega_0^\beta = uq_0 + u\sum_{j=0}^{M} q_j(\hat{h}_j^\beta)'(z_0^\beta)\omega_j^\beta. \quad (20)$$

In matrix notation, equation (18) yields in the inflow case an ODE system like equation (8) with $\mathbf{q} = [q_1,\ldots,q_M]^T$,

$$\mathbf{g} = \omega_0^\beta uq_L\left[\frac{(\hat{h}_0^\beta)'(z_1^\beta)}{\omega_1^\beta},\ldots,\frac{(\hat{h}_0^\beta)'(z_M^\beta)}{\omega_M^\beta}\right]^T \quad (21)$$

and $\mathbf{A} = u\mathbf{\Omega}_M^{-1}(\mathbf{D}_\beta)_M\mathbf{\Omega}_M$, where again $\mathbf{\Omega}_M$ denotes the $M \times M$ diagonal matrix obtained omitting from $\mathbf{\Omega}$ the first row and the first column. In the outflow case instead one has $\mathbf{q} = [q_0,\ldots,q_M]^T$, $\mathbf{g} = \mathbf{0}$ and

$$\mathbf{A} = \frac{u}{\omega_0^\beta}\mathbf{e}_1\mathbf{e}_1^T + u\mathbf{\Omega}^{-1}\mathbf{D}_\beta\mathbf{\Omega}. \quad (22)$$

Examples of eigenvalue plots for $\mathbf{A}$ in the a2n case with GLR nodes are shown in figure 3. It can be seen that the eigenvalue structure is entirely analogous to that of the collocation case a1. This contrasts with the analogous case discretized with GL nodes. Indeed, it can be seen in figure 4 that eigenvalues are much more spread out, with large negative real parts that identify a potentially stiff problem. The situation is even worse for the outflow case (not shown), for which the largest eigenvalue (in absolute value) appears to be of the order 10^{52}.

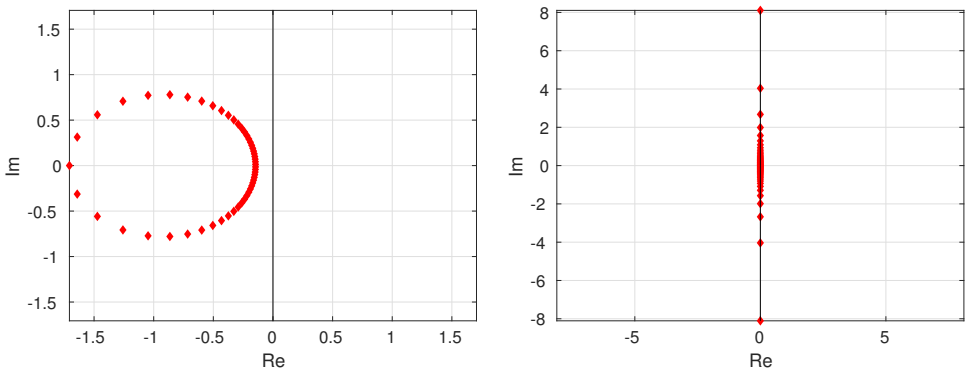

(a) (b)

Figure 3: Eigenvalues in the a2n case with GLR nodes, for parameter values $\beta = 1$, $M = 50$ in the a) outflow case $u = -1$ and b) inflow case $u = 1$.

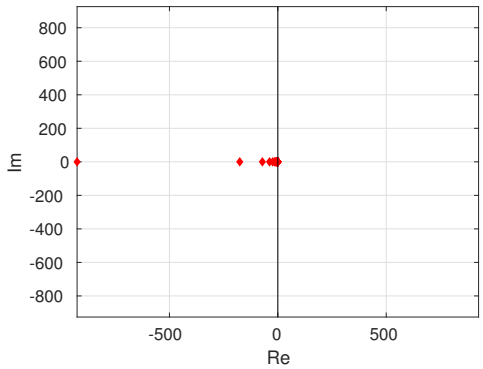

Figure 4: Eigenvalues in the a2n case with GL nodes, for parameter values $\beta = 1$, $M = 50$ in the inflow case $u = 1$.

Weak form, nodal approach with scaled Laguerre polynomials

Using Laguerre polynomials, the expansion (12) reads instead:

$$q(z) \approx \sum_{j=0}^{M} q_j h_j^{\beta}(z). \tag{23}$$

Considering SGL nodes first, and replacing the expression in (6) we find, in the inflow case:

$$\frac{d}{dt}\int_0^{+\infty} h_i^\beta(z)\sum_{j=0}^M q_j h_j^\beta(z)\omega(z)\,dz+\beta u\int_0^{+\infty} h_i^\beta(z)\sum_{j=0}^M q_j h_j^\beta(z)\omega(z)\,dz$$
$$-uq_L h_i^\beta(0)\omega(0)-u\int_0^{+\infty}\left(h_i^\beta\right)'(z)\sum_{j=0}^M q_j h_j^\beta(z)\omega(z)\,dz=0 \quad (24)$$

and in the outflow case, using (7):

$$\frac{d}{dt}\int_0^{+\infty} h_i^\beta(z)\sum_{j=0}^M q_j h_j^\beta(z)\omega(z)\,dz+\beta u\int_0^{+\infty} h_i^\beta(z)\sum_{j=0}^M q_j h_j^\beta(z)\omega(z)\,dz$$
$$-u\sum_{j=0}^M q_j h_j^\beta(0)h_i^\beta(0)\omega(0)-u\int_0^{+\infty}\left(h_i^\beta\right)'(z)\sum_{j=0}^M q_j h_j^\beta(z)\omega(z)\,dz=0 \quad (25)$$

Discretizing the integrals with quadrature formulas based on Laguerre polynomials we get, for $i=0,\dots,M$, in the inflow case:

$$\frac{d}{dt}\sum_{k=0}^M h_i^\beta(z_k^\beta)\sum_{j=0}^M q_j h_j^\beta(z_k^\beta)\omega_k^\beta+\beta u\sum_{k=0}^M h_i^\beta(z_k^\beta)\sum_{j=0}^M q_j h_j^\beta(z_k^\beta)\omega_k^\beta$$
$$-uq_L h_i^\beta(0)\omega(0)-u\sum_{k=0}^M\left(h_i^\beta\right)'(z_k^\beta)\sum_{j=0}^M q_j h_j^\beta(z_k^\beta)\omega_k^\beta=0 \quad (26)$$

and a similar expression for the outflow case upon replacement of q_L with $\sum_{j=0}^M q_j h_j^\beta(0)$. With further simplifications and using also the fact that $\omega(0)=1$, we get for $i=0,\dots,M$ in the inflow case:

$$q_i'\omega_i^\beta=uq_L h_i^\beta(0)-\beta u q_i\omega_i^\beta+u\sum_{j=0}^M q_j(h_j^\beta)'(z_i^\beta)\omega_j^\beta \quad (27)$$

and in the outflow case:

$$q_i'\omega_i^\beta=u\sum_{j=0}^M q_j h_j^\beta(0)h_i^\beta(0)-\beta u q_i\omega_i^\beta+u\sum_{j=0}^M q_j(h_j^\beta)'(z_i^\beta)\omega_j^\beta \quad (28)$$

In matrix form, in the inflow case we have:

$$\mathbf{A}=u\mathbf{\Omega}^{-1}\mathbf{D}_\beta\mathbf{\Omega}-\beta u\mathbf{I},\quad \mathbf{g}=uq_L\mathbf{\Omega}^{-1}\mathbf{h},\quad \mathbf{h}=[h_0(0),\dots,h_M(0)]^T \quad (29)$$

while in the outflow case $\mathbf{g} = 0$ and

$$\mathbf{A} = u\mathbf{\Omega}^{-1}\mathbf{H} + u\mathbf{\Omega}^{-1}\mathbf{D}_\beta\mathbf{\Omega} - \beta u\mathbf{I}. \tag{30}$$

The spectrum of this matrix behaves in a manner that is analogous to the weak form, Laguerre function case shown in figure 4. Also in this case, the eigenvalues in the outflow case become extremely large.

In the case of SGLR nodes, replacing in (6) we find in the inflow case, for $i = 1, \ldots, M$:

$$q_i'\omega_i^\beta = uq_L\left(h_0^\beta\right)'(0)\omega_0^\beta - \beta uq_i\omega_i + u\sum_{j=1}^{M} q_j\left(h_j^\beta\right)'(z_i^\beta)\omega_j^\beta \tag{31}$$

Replacing in (7) we find in the outflow case, for $i = 1, \ldots, M$

$$q_i'\omega_i^\beta = -\beta uq_i\omega_i + u\sum_{j=0}^{M} q_j\left(h_j^\beta\right)'(z_i^\beta)\omega_j^\beta \tag{32}$$

while for $i = 0$ we get:

$$q_0'\omega_0^\beta = uq_0 - \beta uq_0\omega_0 + u\sum_{j=0}^{M} q_j\left(h_j^\beta\right)'(0)\omega_j^\beta. \tag{33}$$

In matrix form, in the inflow case we have, denoting $\mathbf{q} = [q_1, \ldots, q_M]^T$,

$$\begin{aligned}\mathbf{A} &= u\mathbf{\Omega}_M^{-1}\left(\mathbf{D}_\beta\right)_M\mathbf{\Omega}_M - \beta u\mathbf{I}_M,\\ \mathbf{g} &= \omega_0^\beta uq_L\left[\frac{\left(h_0^\beta\right)'(0)}{\omega_1^\beta}, \ldots, \frac{\left(h_0^\beta\right)'(0)}{\omega_M^\beta}\right]^T\end{aligned} \tag{34}$$

In the outflow case, $\mathbf{q} = [q_0, \ldots, q_M]^T$, $\mathbf{g} = 0$ and

$$\mathbf{A} = \frac{u}{\omega_0^\beta}\mathbf{e_1}\mathbf{e_1}^T + u\mathbf{\Omega}^{-1}\mathbf{D}_\beta\mathbf{\Omega} - \beta u\mathbf{I} \tag{35}$$

The spectrum of the matrix $\mathbf{A}$ is depicted in figure 5, the findings are equivalent to the collocation discretization of the model in strong form.

Weak form, modal approach with scaled Laguerre functions

In case a modal discretization based on the scaled Laguerre functions is sought, the solution will instead be represented as

$$q(z) \approx \sum_{j=0}^{M} q_j\hat{\mathscr{L}}_j^\beta(z), \tag{36}$$

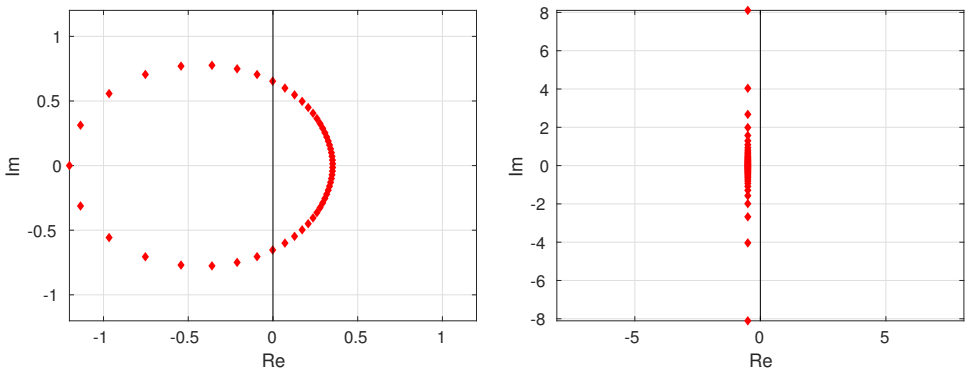

(a) (b)

Figure 5: Eigenvalues in the a2n case with GLR nodes, scaled Laguerre polynomials, for parameter values $\beta = 1$, $M = 50$ in the a) outflow case $u = -1$ and b) inflow case $u = 1$.

where

$$q_j = \beta \int_0^{+\infty} q(z) \hat{\mathscr{L}}_j^\beta(z)\, dz. \tag{37}$$

This implies that, substituting in (3) and choosing $\hat{\mathscr{L}}_i^\beta$ as test function we obtain, in the inflow case,

$$\frac{1}{\beta} q_i' = u q_L + u \sum_{j=0}^{M} q_j \int_0^{+\infty} \frac{\partial}{\partial z} \hat{\mathscr{L}}_i^\beta(z) \hat{\mathscr{L}}_j^\beta(z)\, dz \quad i = 0, \ldots, M, \tag{38}$$

where we have used the fact that $\hat{\mathscr{L}}_i^\beta(0) = 1$. One can then consider that

$$\frac{\partial}{\partial z} \hat{\mathscr{L}}_i^\beta(z) = -\frac{\beta}{2} \hat{\mathscr{L}}_i^\beta(z) - \beta \sum_{k=0}^{i-1} \hat{\mathscr{L}}_k^\beta(z) \tag{39}$$

to obtain

$$\begin{aligned} \sum_{j=0}^{M} q_j \int_0^{+\infty} \frac{\partial}{\partial z} \hat{\mathscr{L}}_i^\beta(z) \hat{\mathscr{L}}_j^\beta(z)\, dz = & -\frac{\beta}{2} \sum_{j=0}^{M} q_j \int_0^{+\infty} \hat{\mathscr{L}}_i^\beta(z) \hat{\mathscr{L}}_j^\beta(z)\, dz \\ & - \beta \sum_{j=0}^{M} q_j \int_0^{+\infty} \hat{\mathscr{L}}_j^\beta(z) \sum_{k=0}^{i-1} \hat{\mathscr{L}}_k^\beta(z)\, dz \\ = & -\frac{q_i}{2} - \sum_{j=0}^{i-1} q_j, \end{aligned} \tag{40}$$

so that in the end we obtain

$$q_i' = \beta u q_L - \beta u \frac{q_i}{2} - \beta u \sum_{j=0}^{i-1} q_j \qquad i = 0, \ldots, M. \tag{41}$$

Going through the same steps after substitution in (4), we obtain for $i = 0, \ldots, M$

$$\frac{1}{\beta} q_i' = u \sum_{j=0}^{M} q_j + u \sum_{j=0}^{M} q_j \int_0^{+\infty} \frac{\partial}{\partial z} \hat{\mathscr{L}}_i^{\beta}(z) \hat{\mathscr{L}}_j^{\beta}(z)\, dz \qquad (42)$$

that simplifies to

$$\begin{aligned} q_i' &= \beta u \sum_{j=0}^{M} q_j - \beta u \frac{q_i}{2} - \beta u \sum_{j=0}^{i-1} q_j \\ &= \beta u \sum_{j=i+1}^{M} q_j + \beta u \frac{q_i}{2} \quad i = 0, \ldots, M. \end{aligned} \qquad (43)$$

In matrix notation, equation (41) yields for the inflow case an ODE system like equation (8) with $\mathbf{q} = [q_0, \ldots, q_M]^T$, $\mathbf{g} = u q_L [1, \ldots, 1]^T$ and $\mathbf{A} = -\beta u \mathbf{L}$, where $\mathbf{L}$ denotes a lower triangular $(M+1)\times(M+1)$ with values equal to one half on the main diagonal and one below. In the outflow case instead one has $\mathbf{q} = [q_0, \ldots, q_M]^T$, $\mathbf{g} = \mathbf{0}$ and $\mathbf{A} = \beta u \mathbf{L}^T$. In both cases, the eigenvalues of the matrix are all equal to $-\beta|u|/2$, so that no stability problems arise.

Weak form, modal approach with scaled Laguerre polynomials

If a modal discretization based on the scaled Laguerre polynomials is sought, one can go through the similar steps as in the previous Sections assuming

$$q(z) \approx \sum_{j=0}^{M} q_j \mathscr{L}_j^{\beta}(z), \qquad (44)$$

and taking into account that the recurrence relationship for the derivatives now reads:

$$\frac{\partial}{\partial z} \mathscr{L}_i^{\beta}(z) = -\beta \sum_{k=0}^{i-1} \mathscr{L}_k^{\beta}(z) \quad \text{for } i \geq 1 \quad \text{and} \quad \frac{\partial}{\partial z} \mathscr{L}_0^{\beta}(z) = 0. \qquad (45)$$

It follows that, for $i \geq 1$,

$$\begin{aligned} &\sum_{j=0}^{M} q_j \int_0^{+\infty} \frac{\partial}{\partial z} \mathscr{L}_i^{\beta}(z) \mathscr{L}_j^{\beta}(z) \omega(z)\, dz = \\ &-\beta \sum_{j=0}^{M} q_j \int_0^{+\infty} \mathscr{L}_j^{\beta}(z) \sum_{k=0}^{i-1} \mathscr{L}_k^{\beta}(z) \omega(z)\, dz = -\sum_{j=0}^{i-1} q_j, \end{aligned} \qquad (46)$$

so that in the end, after substitution in (6), we obtain

$$\frac{1}{\beta}q_0' = uq_L - uq_0 \tag{47}$$

$$\frac{1}{\beta}q_i' = uq_L - uq_i - u\sum_{j=0}^{i-1} q_j = uq_L - u\sum_{j=0}^{i} q_j \qquad i = 1, \ldots, M. \tag{48}$$

Going through the same steps after substitution in (7), we obtain for $i = 0, \ldots, M$

$$\frac{1}{\beta}q_i' = u\sum_{j=0}^{M} q_j - uq_i + u\sum_{j=0}^{M} q_j \int_0^{+\infty} \frac{\partial}{\partial z}\mathscr{L}_i^\beta(z)\mathscr{L}_j^\beta(z)\,dz \tag{49}$$

that simplifies to

$$\frac{1}{\beta}q_0' = u\sum_{j=0}^{M} q_j - uq_0 \tag{50}$$

$$\frac{1}{\beta}q_i' = u\sum_{j=0}^{M} q_j - uq_i - u\sum_{j=0}^{i-1} q_j = u\sum_{j=i+1}^{M} q_j \qquad i = 1, \ldots, M. \tag{51}$$

In matrix notation, equation (48) yields for the inflow case an ODE system like equation (8) with $\mathbf{q} = [q_0, \ldots, q_M]^T$, $\mathbf{g} = uq_L[1, \ldots, 1]^T$ and $\mathbf{A} = -\beta u\mathbf{L}$, where $\mathbf{L}$ denotes a lower triangular $(M+1)\times(M+1)$ matrix with values equal to one on and below the main diagonal. In the outflow case instead one has $\mathbf{q} = [q_0, \ldots, q_M]^T$, $\mathbf{g} = \mathbf{0}$ and $\mathbf{A} = \beta u\mathbf{U}$, where $\mathbf{U}$ denotes an upper triangular $(M+1)\times(M+1)$ matrix with values equal to zero on the main diagonal and one above the main diagonal. In the inflow case, the eigenvalues of the matrix are all equal to $-\beta u$, so that no stability problems arise. In the outflow case, the matrix has all eigenvalues equal to zero, so that again no stability problems arise.

3 A scaled Laguerre functions discretization of hyperbolic systems

In this Section, we present a discretization of hyperbolic systems on semi-infinite domains. Based on the analysis in Section 2, we opt for a weak form discretization with a modal basis of Laguerre scaled functions. In order to account for cases of practical interest in relevant applications, we consider the system

$$\frac{\partial \mathbf{q}}{\partial t} + \mathbf{A}(\mathbf{q}, z)\frac{\partial \mathbf{q}}{\partial z} = \mathbf{B}(\mathbf{q}, z)\mathbf{q}. \tag{52}$$

The system is hyperbolic if, for any $(\mathbf{q}, z)$, the matrix $\mathbf{A}(\mathbf{q}, z) \in \mathbb{R}^d \times \mathbb{R}^d$ is diagonalizable as $\mathbf{A} = \mathbf{V}\mathbf{\Lambda}\mathbf{V}^{-1}$, and has real eigenvalues. The matrix $\mathbf{B}$ represents a zero order forcing term, such as for example the Coriolis force or buoyancy effects in the propagation of internal gravity waves. We first consider equations (52) on the whole domain $\mathbb{R}^+$, written componentwise as

$$\frac{\partial q_k}{\partial t} + \sum_{l=1}^{d} a_{kl}\frac{\partial q_l}{\partial z} = \sum_{l=1}^{d} b_{kl} q_l, \quad k = 1, \ldots, d \tag{53}$$

where a_{kl}, b_{kl} are the entries of $\mathbf{A}$, $\mathbf{B}$, respectively. Notice that the dependency on $\mathbf{q}, z$, has been omitted to simplify the notation. We then define as customary the matrices $\mathbf{A}^{\pm} = \mathbf{V}\mathbf{\Lambda}^{\pm}\mathbf{V}^{-1}$, where $\lambda_i^+ = \max\{\lambda_i, 0\}$, $\lambda_i^- = \min\{\lambda_i, 0\}$. We denote by $g_k(t)$ the value assigned to each component of the system by the Dirichlet boundary conditions and by $\hat{q}_{k,j}, j = 0, \ldots, M$ the $j-$th modal coefficient of q_k, so that each component will be represented as

$$q_k(z, t) \approx \sum_{j=0}^{M} q_{k,j}(t)\hat{\mathscr{L}}_j^{\beta}(z), \tag{54}$$

where

$$q_{k,j} = \beta \int_0^{+\infty} q_k(z)\hat{\mathscr{L}}_j^{\beta}(z)\, dz. \tag{55}$$

Integrating (53) against a test function $\hat{\mathscr{L}}_i^{\beta}$, we have again for $k = 1, \ldots, d$

$$\begin{aligned} \int_0^{+\infty} \frac{\partial q_k}{\partial t}(z, t)\hat{\mathscr{L}}_i^{\beta}(z)\, dz &= -\sum_{l=1}^{d} \int_0^{+\infty} \hat{\mathscr{L}}_i^{\beta}(z) a_{kl}\frac{\partial q_l}{\partial z}(z, t)\, dz \\ &+ \sum_{l=1}^{d} \int_0^{+\infty} \hat{\mathscr{L}}_i^{\beta}(z) b_{kl} q_l(z, t),\, dz. \end{aligned}$$

Since, performing integration by parts, one has

$$\begin{aligned}
&\sum_{l=1}^{d}\int_0^{+\infty}\hat{\mathscr{L}}_i^{\beta}(z)a_{kl}\frac{\partial q_l}{\partial z}(z,t)\,dz\\
&=-\hat{\mathscr{L}}_i^{\beta}(0)\sum_{l=1}^{d}a_{kl}^{+}g_l(t)-\hat{\mathscr{L}}_i^{\beta}(0)\sum_{l=1}^{d}a_{kl}^{-}q_l(0)\\
&-\sum_{l=1}^{d}\int_0^{+\infty}q_l(z,t)a_{kl}\frac{\partial\hat{\mathscr{L}}_i^{\beta}}{\partial z}(z)\,dz\\
&-\sum_{l=1}^{d}\int_0^{+\infty}q_l(z,t)\hat{\mathscr{L}}_i^{\beta}(z)\frac{\partial a_{kl}}{\partial z}(z)\,dz\\
&+\sum_{l=1}^{d}\int_0^{+\infty}\hat{\mathscr{L}}_i^{\beta}(z)b_{kl}q_l(z,t),\,dz. \qquad (56)
\end{aligned}$$

using the fact that $\hat{\mathscr{L}}_i^{\beta}(0)=1$ it follows

$$\begin{aligned}
\frac{1}{\beta}\frac{d}{dt}q_{k,i}(t) \;=\;& \sum_{l=1}^{d}a_{kl}^{+}g_l(t)+\sum_{l=1}^{d}a_{kl}^{-}\sum_{j=0}^{M}q_{l,j}(t)\\
&+\sum_{l=1}^{d}\int_0^{+\infty}q_l(z,t)a_{kl}\frac{\partial\hat{\mathscr{L}}_i^{\beta}}{\partial z}(z)\,dz\\
&+\sum_{l=1}^{d}\int_0^{+\infty}q_l(z,t)\hat{\mathscr{L}}_i^{\beta}(z)\frac{\partial a_{kl}}{\partial z}(z)\,dz\\
&+\sum_{l=1}^{d}\int_0^{+\infty}\hat{\mathscr{L}}_i^{\beta}(z)b_{kl}q_l(z,t)\,dz. \qquad (57)
\end{aligned}$$

Using formulae (39) and (54) one obtains then

$$\begin{aligned}\frac{1}{\beta}\frac{d}{dt}q_{k,i}(t) &= \sum_{l=1}^{d} a_{kl}^{+} g_l(t) + \sum_{l=1}^{d} a_{kl}^{-} \sum_{j=0}^{M} q_{l,j}(t) \\ &\quad -\frac{\beta}{2}\sum_{l=1}^{d}\sum_{j=0}^{M} q_{l,j}(t) \int_0^{+\infty} a_{kl}\hat{\mathscr{L}}_i^{\beta}(z)\hat{\mathscr{L}}_j^{\beta}(z)\,dz \\ &\quad -\beta\sum_{l=1}^{d}\sum_{j=0}^{M} q_{l,j}(t) \sum_{s=0}^{i-1} \int_0^{+\infty} a_{kl}\hat{\mathscr{L}}_s^{\beta}(z)\hat{\mathscr{L}}_j^{\beta}(z)\,dz \\ &\quad +\sum_{l=1}^{d}\sum_{j=0}^{M} q_{l,j}(t) \int_0^{+\infty} \hat{\mathscr{L}}_i^{\beta}(z)\hat{\mathscr{L}}_j^{\beta}(z)\frac{\partial a_{kl}}{\partial z}(z)\,dz \\ &\quad +\sum_{l=1}^{d}\sum_{j=0}^{M} q_{l,j}(t) \int_0^{+\infty} b_{kl}\hat{\mathscr{L}}_i^{\beta}(z)\hat{\mathscr{L}}_j^{\beta}(z)\,dz. \qquad (58)\end{aligned}$$

In the linear, constant coefficient case, the integrals in (58) yield expressions similar to those derived in Section 2, while in the variable coefficient or nonlinear case a full space discretization is obtained by applying the Gauss - Laguerre - Radau quadrature formulae.

4 Coupling of the scaled Laguerre discretization with a DG discretization on the finite domain

We now split the domain $\mathbb{R}^+$ as $\mathbb{R}^+ = [0, L] \cup [L, +\infty)$ in order to introduce two different discretizations on the finite and semi-infinite parts of the domain. On $[L, +\infty)$, system (53) is discretized by (58), where an appropriate shift is performed in the independent variable.

On the finite domain, a DG discretization is employed. For definiteness, we have applied here a modal DG approach. More specifically, a computational mesh is introduced in the $[0, L]$ interval by defining a set of N non overlapping elements K_m of size Δz_m, such that $[0, L] = \bigcup_{m=1}^{N} K_m$. The center of the generic element K_m is denoted by z_m, while $z_{m\pm 1/2}$ denote its boundary points. Each element K_m can be seen as the image of the master element $\hat{K} = [-1, 1]$ via the affine local map $z = f_m(\xi) = \xi\Delta z_m/2 + z_m$, where $z \in K_m$ and $\xi \in \hat{K}$. For each non-negative integer p, we then denote by $\mathbb{P}_p$ the set of all polynomials of degree less or equal to p on $\hat{K}$. We will also define $\mathbb{P}_p(K_m) = \left\{w : w = v \circ F_m^{-1}, \quad v \in \mathbb{P}_p\right\}$. For each polynomial degree p, the discontinuous finite element spaces are defined

as follows

$$V_h^p = \left\{ v \in L^2([0,L]) : v|_{K_m} \in \mathbb{P}_p(K_m) \quad m = 1, \ldots, N \right\}, \tag{59}$$

For each element K_m, $m = 1, \ldots, N$ we then denote by $\phi_j^m(z), j = 0, \ldots, p$ a basis of $\mathbb{P}_p(K_m)$. For discontinuous finite elements discretizations, we will consider instead the orthogonal basis based on Legendre polynomials. More specifically, for $\xi \in \hat{K}$, define the Legendre polynomial recursively by the following recurrence relation:

$$\begin{aligned} &L_{k+1} = \frac{2k+1}{k+1}\xi L_k(\xi) - \frac{k}{k+1}L_{k-1}(\xi), \quad k = 1, 2, \ldots \\ &L_0(\xi) = 1, \qquad L_1(\xi) = \xi. \end{aligned} \tag{60}$$

The Legendre polynomials form an orthogonal basis for polynomials on $\hat{K}$ since

$$\int_{-1}^{1} L_p(\xi) L_q(\xi) d\xi = \frac{2}{2p+1}\delta_{pq}. \tag{61}$$

This orthogonality property of basis functions implies that the mass matrices are diagonal and gives improved conditioning to the resulting discretization. In particular, we will use basis functions

$$\phi_l^m(z) = \sqrt{2l+1} L_l\Big(2\frac{z - z_m}{\Delta z_m}\Big), \tag{62}$$

which are normalized so that

$$\int_{z_{m-\frac{1}{2}}}^{z_{m+\frac{1}{2}}} \phi_p^m(z)\phi_q^m(z)\, dz = \Delta z_m \delta_{pq}. \tag{63}$$

Therefore, each component of the solution of (53) will be represented as

$$q_k(z,t) \approx \sum_{j=0}^{p} q_{k,m}^{(j)}(t)\phi_j^m(z), \qquad z \in K_m. \tag{64}$$

Integrating (53) against a test function $\phi_i^m(z)$ on K_m one obtains for $k = 1, \ldots, d$, $i = 1, \ldots, N$ and $m = 0, \ldots, p$

$$\begin{aligned} \int_{z_{m-\frac{1}{2}}}^{z_{m+\frac{1}{2}}} \frac{\partial q_k}{\partial t}\phi_i^m(z)\, dz &= -\sum_{l=1}^{d} \int_{z_{m-\frac{1}{2}}}^{z_{m+\frac{1}{2}}} a_{kl}\frac{\partial q_l}{\partial z}\phi_i^m(z)\, dz \\ &+ \sum_{l=1}^{d} \int_{z_{m-\frac{1}{2}}}^{z_{m+\frac{1}{2}}} b_{kl} q_l(z,t)\phi_i^m(z)\, dz. \end{aligned} \tag{65}$$

In the linear, constant coefficient case a full spatial semi-discretization is obtained then by substituting (64), performing standard integration by parts and introducing numerical fluxes, see e.g. [8]. In the variable coefficient or nonlinear case, the double integration by part technique proposed in [4] (see also [35]) is employed to handle the non conservative product, as well as numerical integration of the resulting integrals by an appropriate quadrature rule.

The discrete equations derived from (65) will require the knowledge of the approximate value of $\lim_{z\to L^+} q(z,t)$, which will be provided by the semi-infinite Laguerre approximation $\sum_{j=0}^{M} q_{l,j}(t)$. Analogously, the boundary condition terms $g_l(t)$ in (58) will be provided by the DG approximation $\sum_{j=0}^{p} q_{k,N}^{(j)}(t)\phi_j^N(L)$. In this way, a seamless integration of the two approaches is achieved.

As the focus of the present work is on spatial discretization aspects, for the sake of simplicity the numerical tests of the algorithms described above are performed with a simple explicit time discretization. Writing the discrete equations resulting from (58), (65) as a single ODE system

$$\frac{d}{dt}\mathbf{q} = \mathbf{f}(t, \mathbf{q}(t)) \tag{66}$$

we divide the simulation interval $[0, T]$ into a succession of time instants $0 = t^0, t^1, \ldots, t^{N_t} = T$, with $t^{n+1} = t^n + \Delta t$ and Δt the time step, assumed constant. Denoting the approximate solution of (66) with $\mathbf{q}^n \approx \mathbf{q}(t^n)$, we use the third-order Runge-Kutta scheme [21]:

$$\mathbf{q}^{n+1} = \mathbf{q}^n + \frac{\Delta t}{6}\left(\mathbf{K}_1 + \mathbf{K}_2 + 4\mathbf{K}_3\right) \tag{67}$$

$$\mathbf{K}_1 = \mathbf{f}\left(t^n;\, \mathbf{q}^n\right); \tag{68}$$

$$\mathbf{K}_2 = \mathbf{f}\left(t^n + \Delta t;\, \mathbf{q}^n + \Delta t\mathbf{K}_1\right); \tag{69}$$

$$\mathbf{K}_3 = \mathbf{f}\left(t^n + \frac{\Delta t}{2}; \mathbf{q}^n + \frac{\Delta t}{4}\left(\mathbf{K}_1 + \mathbf{K}_2\right)\right) \tag{70}$$

A semi-implicit time discretization stategy will be considered in future multi-dimensional extensions of this paper.

5 Numerical experiments

In this Section we report the results of numerical tests with the coupled DG-Laguerre model described in Section 4. In view of the results of the analysis, we will consider a weak modal discretization based on scaled Laguerre functions with GLR quadrature in the

semi-infinite domain. Linear polynomials will be used for the modal DG scheme in the finite domain.

The coupled scheme will be tested on the case of the shallow water equations and the suite of tests of [6]. The accuracy of the coupling strategy will be verified by sending signals from either side of the interface between the finite and semi-infinite domain and evaluating the solution by comparison with a modal DG discretization on a single domain of the same extension as the coupled model. As in [6], a large number of modes will be used in the semi-infinite part for this first test in order to identify the coupling error.

By using a damping term in the semi-infinite part, the coupled model will be used to simulate an absorbing layer, with the aim to show that outgoing waves can be accurately and efficiently dissipated with minimal reflections into the finite region. To this end the model will initially be run with a long lead time and a non homogeneous wavetrain inflow boundary condition in the finite domain, again comparing the final result with a single-domain discretization. Next, the efficiency of the absorbing layer will be tested by lowering the number of spectral modes and assessing the amplitude of reflected signals in tests with Gaussian initial data.

The equations governing the small perturbations of a free surface of a nonrotating fluid of height h and velocity u under constant gravity for $z \in \mathbb{R}^+ = [0, +\infty]$ are:

$$\frac{\partial h}{\partial t} + U\frac{\partial h}{\partial z} + H\frac{\partial u}{\partial z} + \gamma h = 0 \tag{71}$$

$$\frac{\partial u}{\partial t} + g\frac{\partial h}{\partial z} + U\frac{\partial u}{\partial z} + \gamma u = 0 \tag{72}$$

together with initial data and boundary conditions. H and U are respectively the reference height and velocity, and g is the acceleration of gravity. Moreover, a Rayleigh damping term with coefficient γ is included. The system (71)-(72) can be derived from the compressible fluid flow equations with the assumption of small aspect ratio of vertical and horizontal length scales [12].

Coupling validation test

The first test uses a motionless Gaussian initial distribution for the height, $h(x,0) = h_1 \exp[(x - x_0)/\sigma]$, where we set $h_1 = 0.1\,\mathrm{m}$ and consider two choices of $\sigma = 500, 1000\,\mathrm{m}$. The number of modes in the semi-infinite domain is $N = 180$, and $\beta = 1/400$, so that the last GLR point is at $x_N = 2.86\mathrm{E}05\,\mathrm{m}$. The absorbing layer is not active, $\gamma = 0$. We consider a $10000\,\mathrm{m}$-wide finite domain, with $N_x = 1250$ cells. We then distinguish the cases of an ingoing wave,

$x_0 = 12000\,\mathrm{m}$, and an outgoing wave, $x_0 = 5000\,\mathrm{m}$. The initial datum splits in two crests and the leftmost one travels through the interface between the finite and semi-infinite domain. The solution of the coupled model is compared on the finite domain with a reference solution obtained with a full DG discretization over 20 km using the same spatial resolution and number of time steps $N_t = 2200$ (Figure 6). As a large number of modes is used in the semi-infinite domain, the relative errors in the finite domain $[0,\ 10]\,\mathrm{km}$ between the multidomain and the single domain schemes (Table 1) identify the residual perturbations coming from the coupling approximation at the interface. Similarly to [6], the errors are at most around a few percent. In a second test, the initial datum is placed inside the

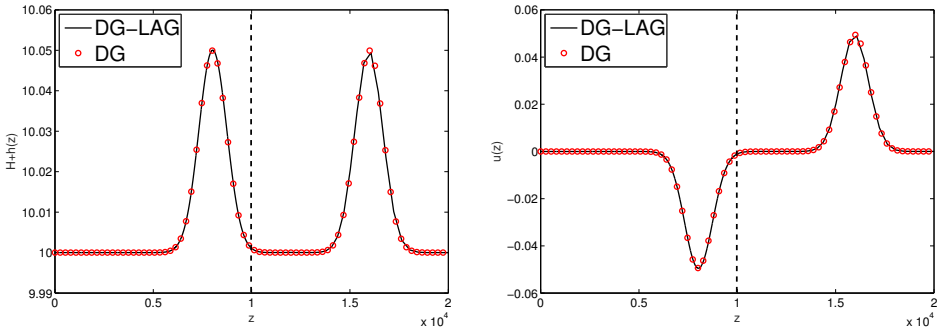

Figure 6: Computed final height (left) and velocity (right) by the coupled DG-Laguerre scheme (solid black line) and single-domain DG scheme (red dots) in the coupling validation, ingoing wave test, $A = 0.1\,\mathrm{m}$, $\sigma = 1000\,\mathrm{m}$.

Table 1: Computed 1-norm ($\mathcal{E}_1$), 2-norm ($\mathcal{E}_2$), and maximum ($\mathcal{E}_\infty$) errors for the coupling validation experiment, ingoing wave (top four rows, relative errors) and outgoing wave (bottom four rows, absolute errors) cases.

x_0	$\tilde{h}$	σ	$\mathcal{E}_1(\eta)$	$\mathcal{E}_1(\mathbf{u})$	$\mathcal{E}_2(\eta)$	$\mathcal{E}_2(\mathbf{u})$	$\mathcal{E}_\infty(\eta)$	$\mathcal{E}_\infty(\mathbf{u})$
12000	0.1	1000	7.37E-03	7.37E-03	8.49E-03	8.48E-03	1.10E-02	1.10E-02
12000	0.1	500	1.58E-02	1.57E-02	1.70E-02	1.70E-02	1.96E-02	1.96E-02
12000	0.5	1000	3.67E-02	3.65E-02	4.14E-02	4.12E-02	5.11E-02	5.09E-02
12000	0.5	500	7.81E-02	7.78E-02	8.33E-02	8.30E-02	8.57E-02	8.54E-02
5000	0.1	1000	3.88E-06	3.84E-06	9.23E-06	9.14E-06	3.11E-05	3.08E-05
5000	0.1	500	1.94E-06	1.92E-06	6.52E-06	6.46E-06	3.11E-05	3.08E-05
5000	0.5	1000	9.36E-05	9.27E-05	2.23E-04	2.21E-04	7.58E-04	7.50E-04
5000	0.5	500	4.68E-05	4.64E-05	1.58E-04	1.56E-04	7.58E-04	7.50E-04

finite domain and run for $N_t = 8400$ time steps until a final time $T = 1000\,\mathrm{s}$ when all perturbations have left the finite domain. Since

the solution in the finite domain is the absence of perturbations in the finite domain, absolute errors with respect to the reference are computed in this case (bottom rows in Table 1). The residual perturbations in the finite domain have negligible amplitude. While a one-to-one comparison with [6], which coupled two fully nonlinear discretizations, is not possible here, the obtained errors appear small enough to test the coupled DG-Laguerre scheme to simulate absorbing layers. Notice that here a different (and more accurate) time discretization method is employed with respect to [6]. Next, we test the coupled scheme with $\gamma \neq 0$ in the semi-infinite domain. As in [6], the damping coefficient will have the sigmoid-like functional form:

$$\gamma(x) = \frac{\Delta\gamma}{1 + \exp\left(\dfrac{\alpha L_0 - x}{\sigma}\right)} \tag{73}$$

where $\Delta\gamma$ is the sigmoid amplitude, L_0 a length scale, typically the absorbing layer thickness, α the position of the sigmoid inside the absorbing layer, and σ the sigmoid steepness, see also Figure 8 in [6], to which we refer for a complete definition of the parameter values employed.

A Dirichlet boundary condition on the velocity is imposed in $x = 0$: $u(0, t) = A \sin(2\pi k/T)$. The initial condition is motionless, with $h(0) = 0$. With these choices, a train of waves with uniform amplitude is generated and propagated through the 5 km-wide finite domain. Once the waves cross the interface, they are damped in the semi-infinite domain that acts as an absorbing layer. In this context, excessive spurious signals coming from the interface would propagate and pollute the wavetrain in the finite domain. We compare again the solution of the coupled model with the one obtained with a DG scheme over a larger domain, with $N = 30$ or $N = 15$ modes in the semi-infinite domain and a longer final time $T = 5000$ s, with two choices for the wavenumber, $k = 30,\ 15\,\mathrm{m}^{-1}$ and three choices for the amplitude, $A = 0.025,\ 0.05,\ 0.1$ m. The case provides a simplified representation of gravity wave propagation in the atmosphere. The obtained relative errors on height and velocity as well as the energy errors:

$$\mathcal{E}_{EN} = \frac{1}{N_x} \sum_i \frac{1}{2} \left[g(h_i - [h_{\mathrm{ref}}]_i)^2 + H(u_i - [u_{\mathrm{ref}}]_i)^2 \right]. \tag{74}$$

are low for all configurations (Figures 7 and 8 and Tables 2 and 3) and in line with the results in [6]. For the evaluation of these results, we note that the Dirichlet condition was imposed on the discharge

in [6] so results obtained with, for instance, $A = 0.2\,\mathrm{m}$ in the present paper should be compared to results with $A(H+\eta) \approx 2\,\mathrm{m}$ of [6].

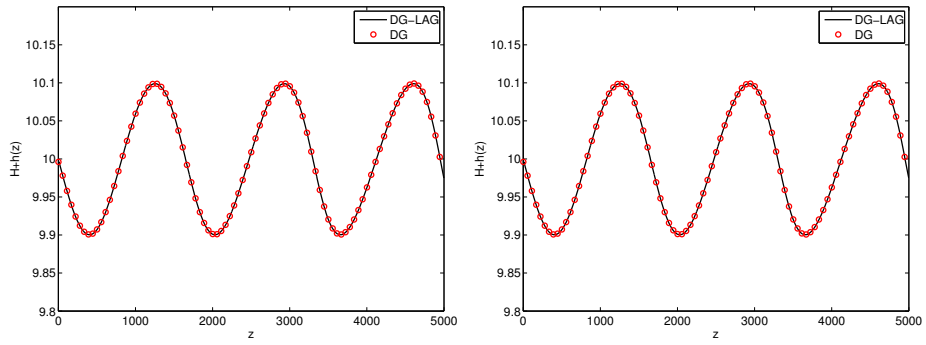

Figure 7: Computed total depth after $T = 5000\,\mathrm{s}$ in the wavetrain test for the coupled DG-Laguerre (solid line) and single-domain DG model (red circles), with 30 (left) and 15 (right) semi-infinite nodes, $A = 0.05\,\mathrm{m}$, $k = 30\,\mathrm{m}^{-1}$.

Table 2: Relative mean square root and maximum errors for elevation η and velocity $\mathbf{u}$ for the wavetrain test, 30 nodes in the semi-infinite domain. See text for other parameters.

A	k	N_x	β	$\mathcal{E}_2^{\mathrm{rel}}(\eta)$	$\mathcal{E}_\infty^{\mathrm{rel}}(\eta)$	$\mathcal{E}_2^{\mathrm{rel}}(\mathbf{u})$	$\mathcal{E}_\infty^{\mathrm{rel}}(\mathbf{u})$	$\mathcal{E}_{\mathrm{EN}}$
0.025	30	600	0.0143	3.84E-06	4.40E-04	6.23E-06	6.10E-04	8.38E-09
0.025	60	1200	0.0286	3.89E-06	6.50E-04	6.03E-06	8.10E-04	9.94E-09
0.05	30	600	0.0143	1.67E-05	8.88E-04	2.72E-05	1.46E-03	1.55E-07
0.05	60	1200	0.0286	2.54E-05	1.19E-03	5.41E-05	2.14E-03	3.51E-07
0.1	30	600	0.0143	1.01E-04	1.98E-03	1.66E-04	5.22E-03	5.41E-06
0.1	60	1200	0.0286	1.32E-04	5.08E-03	1.50E-03	6.71E-02	1.11E-05

In the final test of the suite of [6], we evaluate the performance of the coupled model in absorbing signals leaving the finite domain. By using a small number of nodes in the semi-infinite domain, the objective is to show that outgoing waves can be efficiently damped and that reflected signals at the interface have low amplitude. As in Section 5 above, we consider a $D = 10\,\mathrm{km}$-wide domain and a Gaussian perturbation centred in $x_0 = 7500\,\mathrm{m}$ with amplitude $\sigma = 500\,\mathrm{m}$. In this case we run the coupled model until the final time $T = D/(2\sqrt{gH})$, at which reflected perturbations will have come back to x_0. We consider the same performance measures as in [6]: residual maximum values for free-surface elevation and velocity, mean square root energy error, and reflection ratio, defined as:

$$\rho = \sqrt{\frac{\mathcal{E}_{EN}(T)}{\mathcal{E}_{EN}^{W}(T)}} \tag{75}$$

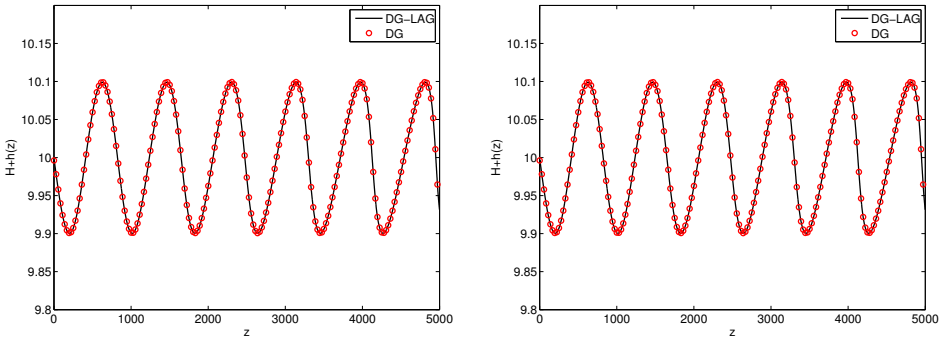

Figure 8: Computed total depth after $T = 5000\,\mathrm{s}$ in the wavetrain test for the coupled DG-Laguerre (solid line) and single-domain DG model (red circles), with 30 (left) and 15 (right) semi-infinite nodes, $A = 0.05\,\mathrm{m}$, $k = 60\,\mathrm{m}^{-1}$.

Table 3: Relative mean square root and maximum errors for elevation η and velocity $\mathbf{u}$ for the wavetrain test, 15 nodes in the semi-infinite domain. See text for other parameters.

A	k	N_x	β	$\mathcal{E}_2^{\mathrm{rel}}(\eta)$	$\mathcal{E}_\infty^{\mathrm{rel}}(\eta)$	$\mathcal{E}_2^{\mathrm{rel}}(\mathbf{u})$	$\mathcal{E}_\infty^{\mathrm{rel}}(\mathbf{u})$	$\mathcal{E}_{\mathrm{EN}}$
0.025	30	600	0.0286	3.80E-06	4.37E-04	6.17E-06	6.07E-04	8.22E-09
0.025	60	1200	0.0571	6.84E-06	5.34E-04	2.27E-05	2.64E-03	2.47E-08
0.05	30	600	0.0286	1.65E-05	8.83E-04	2.70E-05	1.45E-03	1.53E-07
0.05	60	1200	0.0571	3.68E-05	1.38E-03	1.13E-04	7.21E-03	7.09E-07
0.1	30	600	0.0286	1.01E-04	1.97E-03	1.66E-04	5.21E-03	5.36E-06
0.1	60	1200	0.0571	1.98E-04	9.59E-03	2.49E-03	1.12E-01	2.82E-05

where $\mathcal{E}_{EN}^W$ denotes the energy error obtained with a solid wall boundary condition at the interface. Results with the DG-Laguerre coupled model are in line or lower than the ones obtained in [6] with a finite volume discretization in the finite domain (Tables 4 and 5).

6 Conclusions and perspectives

We analyzed the stability of Laguerre spectral discretizations of hyperbolic problems on semi-infinite domains, by computing the spectra for the strong and weak, nodal and modal discretization of the linear advection equation based on Laguerre polynomials and functions with a range of options for boundary conditions and quadrature rules. Discretizations using Gauss-Laguerre-Radau quadrature nodes and scaled Laguerre functions were found to give the best results in terms of stability, while the analysis rules out the use of Laguerre polynomials due to their poor stability properties. To the

Table 4: Maximum residual elevation, velocity, mean square root energy error and reflection ratios for the single Gaussian perturbation test, coupled DG/Laguerre scheme.

N	N_x	$T/\Delta t$	$\|\eta(T)\|_\infty$	$\|u(T)\|_\infty$	$\mathcal{E}_{\text{EN}}$	ρ
40	400	600	2.92E-03	2.90E-03	7.23E-06	4.57E-03
30	300	450	2.91E-03	2.88E-03	7.17E-06	4.55E-03
20	200	300	3.00E-03	2.97E-03	7.27E-06	4.58E-03
10	100	150	3.13E-03	3.11E-03	8.16E-06	4.88E-03

Table 5: Further reflection ratios for the single Gaussian perturbation test, coupled DG/Laguerre scheme.

N	N_x	$T/\Delta t$	β	ρ
40	400	600	1/280	4.57E-03
30	400	600	1/210	4.57E-03
20	400	600	1/145	4.56E-03
10	400	600	1/75	4.56E-03
5	400	600	1/40	4.05E-03
30	300	450	1/280	4.55E-03
20	300	450	1/190	4.54E-03
10	300	450	1/110	4.52E-03
5	300	450	1/40	4.12E-03
20	200	300	1/280	4.58E-03
10	200	300	1/120	4.52E-03
5	200	300	1/55	4.21E-03
13	110	150	1/270	4.80E-03
5	110	150	1/250	5.03E-03

best of our knowledge, this is the first analysis of this kind in the literature on spectral methods for fluid dynamics.

The theory was then extended to systems of equations, and a modal semi-infinite discretization was coupled with a discontinuous finite element scheme in a finite domain. The resulting scheme was tested on the propagation of single wave and wavetrains, with outcomes on validation and absorbing layer efficiency tests in line with the findings in [6]. Therefore, the scaled Laguerre approach in the unbounded region was effectively shown to work independently of the form of the discretization in the finite domain.

The results suggest the potential of the Laguerre spectral discretization as a flexible and independent tool to accurately simulate wave propagation on unbounded domains, as well as to reduce the computational cost of absorbing unwanted perturbations without spurious reflections. In particular, extensions to nonlinear systems can be considered in multiple space dimensions via tensor-product approaches in the unbounded domain and continuous, discontinu-

ous, or mixed finite element discretizations in the bounded domain [9]. Due to the variety of interacting solutions in full-fledged numerical weather prediction systems, the flexibility of the scaled spectral absorbing layer could be productively employed to lower the cost of standard approaches currently deployed in operational models.

Acknowledgements

We kindly acknowledge useful discussions on the topics of this paper with Vadym Aizinger. The contribution of T.B. is covered by ©Crown Copyright 2018. L.B. gratefully acknowledges the financial support from the Met Office for a visit in May 2015, in which the work on this paper was started.

References

[1] S. Abarbanel, D. Gottlieb, and J.S. Hesthaven. Well-posed perfectly matched layers for advective acoustics. *Journal of Computational Physics*, 154:266–283, 1999.

[2] D. Appelö and T. Colonius. A high-order super-grid-scale absorbing layer and its application to linear hyperbolic systems. *Journal of Computational Physics*, 228(11):4200–4217, 2009.

[3] R.J. Astley. Infinite elements for wave problems: a review of current formulations and an assessment of accuracy. *International Journal for Numerical Methods in Engineering*, 49(7):951–976, 2000.

[4] F. Bassi and S. Rebay. High Order Accurate Discontinuous Finite Element Method for the Numerical Solution of the Compressible Navier-Stokes Equations. *Journal of Computational Physics*, 131:267–279, 1997.

[5] T. Benacchio. Spectral collocation methods on semi–infinite domains and application to open boundary conditions. Master's thesis, Politecnico di Milano, 2010.

[6] T. Benacchio and L. Bonaventura. Absorbing boundary conditions: a spectral collocation approach. *International Journal for Numerical Methods in Fluids*, 72(9):913–936, 2013.

[7] J.-P. Berenger. A perfectly matched layer for the absorption of electromagnetic waves. *Journal of Computational Physics*, 114:185–200, 1994.

[8] B. Cockburn and S.Y. Lin. TVB Runge-Kutta local projection discontinuous Galerkin finite element method for conservation laws III: one dimensional systems. *Journal of Computational Physics*, 84:90–113, 1989.

[9] C. J Cotter and J. Shipton. Mixed finite elements for numerical weather prediction. *Journal of Computational Physics*, 231(21):7076–7091, 2012.

[10] J.-R. Dea, F.-X. Giraldo, and B. Neta. High-order non-reflecting boundary conditions for the linearized 2-d euler equations: no mean flow case. *Wave Motion*, 46:210–220, 2009.

[11] J.R. Dea. An experimental adaptation of higdon-type non-reflecting boundary conditions to linear first-order systems. *Journal of Computational and Applied Mathematics*, 235:1354–1366, 2011.

[12] A. Decoene, L. Bonaventura, E. Miglio, and F. Saleri. Asymptotic derivation of the section averaged shallow water equations for natural river hydraulics. *Mathematical Models and Methods in Applied Sciences*, 19:387–417, 2009.

[13] D.R. Durran, M.O.G. Hills, and P.N. Blossey. The dissipation of trapped lee waves. Part I: Leakage of inviscid waves into the stratosphere. *Journal of the Atmospheric Sciences*, 72(4):1569–1584, 2015.

[14] D.R. Durran and J.B. Klemp. A Compressible Model for the Simulation of Moist Mountain Waves. *Monthly Weather Review*, 111:2341–2361, 1983.

[15] B. Engquist and A. Majda. Absorbing boundary conditions for numerical simulation of waves. *Mathematics of Computation*, 31(139):629–651, 1977.

[16] K. Gerdes. A review of infinite element methods for exterior Helmholtz problems. *Journal of Computational Acoustics*, 8(1):43–62, 2000.

[17] M.A. Giorgetta, E. Manzini, E. Roeckner, M. Esch, and L. Bengtsson. Climatology and forcing of the quasi–biennal oscillation in the MAECHAM5 model. *Journal of Climate*, 19(16):3882–3901, 2006.

[18] D. Givoli. Computational Absorbing Boundaries. In S. Marburg and B. Nolte, editors, *Computational Acoustics of Noise Propagation in Fluids – Finite and Boundary Element Methods*. Springer Berlin Heidelberg, 2008.

[19] J.S. Hesthaven. On the analysis and construction of perfectly matched layers for the linearized euler equations. *Journal of Computational Physics*, 142:129–147, 1998.

[20] T. Horinouchi, S. Pawson, K. Shibata, U. Langematz, E. Manzini, M.A. Giorgetta, F. Sassi, R.J. Wilson, K. Hamilton, J. De Grandpré, and A.A. Scaife. Tropical cumulus convection and upward–propagating waves in middle–atmospheric GCMs. *Journal of the Atmospheric Sciences*, 60(22):2765–2782, 2003.

[21] W. Hundsdorfer, B. Koren, M. van Loon, and J.G. Verwer. A positive finite-difference advection scheme. *Journal of Computational Physics*, 117(1):35–46, 1995.

[22] M. Israeli and S.A. Orszag. Approximation of Radiation Boundary Conditions. *Journal of Computational Physics*, 41:115–135, 1981.

[23] J.B. Klemp, J. Dudhia, and A.D. Hassiotis. An Upper Gravity–Wave Absorbing Layer for NWP Applications. *Monthly Weather Review*, 136(10):3987–4004, 2008.

[24] J.B. Klemp and D.K. Lilly. Numerical Simulation of Hydrostatic Mountain Waves. *Journal of the Atmospheric Sciences*, 35:78–107, 1978.

[25] J.W. Lavelle and W.C. Thacker. A pretty good sponge: Dealing with open boundaries in limited–area ocean models. *Ocean Modelling*, 20(3):270–292, 2008.

[26] A. Modave, É. Deleersnijder, and É.J.M. Delhez. On the parameters of absorbing layers for shallow water models. *Ocean Dynamics*, 60:65–79, 2010.

[27] A. Modave, J. Lambrechts, and C. Geuzaine. Perfectly matched layers for convex truncated domains with discontinuous Galerkin time domain simulations. *Computers & Mathematics with Applications*, 73(4):684–700, 2017.

[28] I.M. Navon, B. Neta, and M. Y. Hussaini. A perfectly matched layer approach to the linearized shallow water equations models. *Monthly Weather Review*, 132(6):1369–1378, 2004.

[29] B. Neta, V. Van Joolen, J.R. Dea, and D. Givoli. Application of high-order higdon non-reflecting boundary conditions to linear shallow water models. *Communications in Numerical Methods in Engineering*, 24(11):1459–1466, 2008.

[30] D. Rabinovich, D. Givoli, J. Bielak, and T. Hagstrom. The double absorbing boundary method for elastodynamics in homoge-

neous and layered media. *Advanced Modeling and Simulation in Engineering Sciences*, 2(1):3, 2015.

[31] P.J. Rasch. Toward atmospheres without tops: Absorbing upper boundary conditions for numerical models. *Quarterly Journal of the Royal Meteorological Society*, 112:1195–1218, 1986.

[32] J. Shen. Stable and efficient spectral methods in unbounded domains using Laguerre functions. *SIAM Journal on Numerical Analysis*, 38:1113–1133, 2001.

[33] J. Shen and L.-L. Wang. Some recent advances on spectral methods for unbounded domains. *Communications in Computational Physics*, 5:195–241, 2009.

[34] S. V. Tsynkov. Numerical solution of problems on unbounded domains. A review. *Applied Numerical Mathematics*, 27:465–532, 1998.

[35] G. Tumolo and L. Bonaventura. A semi-implicit, semi-Lagrangian, DG framework for adaptive numerical weather prediction. *Quarterly Journal of the Royal Meteorological Society*, 141:2582–2601, 2015.

[36] Z.-Q. Wang, B.-Y. Guo, and Y.-N. Wu. Pseudospectral method using generalized Laguerre functions for singular problems on unbounded domains. *Discrete and Continuous Dynamical Systems - Series B*, 11(4):1019–1038, 2009.

[37] B. Yang and J.S. Hesthaven. A pseudospectral method for time-domain computation of electromagnetic scattering by bodies of revolution. *IEEE Transactions on Antennas and Propagation*, 47(1):132–141, 1999.

[38] Q. Zhuang, J. Shen, and C. Xu. A coupled Legendre–Laguerre spectral–element method for the Navier–Stokes equations in unbounded domains. *Journal of Scientific Computing*, 42(1):1–22, 2010.

MOX Technical Reports, last issues

Dipartimento di Matematica
Politecnico di Milano, Via Bonardi 9 - 20133 Milano (Italy)

21/2018 Gervasio, P.; Dede', L.; Chanon, O.; Quarteroni, A.
Comparing Isogeometric Analysis and Spectral Element Methods: accuracy and spectral properties

22/2018 Pegolotti, L.; Dede', L.; Quarteroni, A.
Isogeometric Analysis of the electrophysiology in the human heart: numerical simulation of the bidomain equations on the atria

20/2018 Bassi, C. ; Abbà, A.; Bonaventura L.; Valdettaro, L.
A priori tests of a novel LES approach to compressible variable density turbulence

19/2018 Menghini, F.; Dede', L.; Quarteroni, A.
Variational Multiscale LES modeling of blood flow in an idealized left human heart

18/2018 Antonietti, P.F.; Bonaldi, F.; Mazzieri, I.
A high-order discontinuous Galerkin approach to the elasto-acoustic problem

17/2018 Agosti, A.; Giverso, C.; Faggiano, E.;Stamm,A.; Ciarletta, P.
A personalized mathematical tool for neuro-oncology: a clinical case study

16/2018 Calissano, A.; Vantini, S.; Arnaboldi, M.
An elephant in the room: Twitter samplingmethodology.

15/2018 Simona, A.; Bonaventura, L.; Pugnat, T.; Dalena, B.
High order time integrators for the simulation of charged particle motion in magnetic quadrupoles

14/2018 Cuffaro, M.; Miglio, E.; Penati, M.;Viganò, M.
Mantle upwelling driven by asymmetric sea-floor spreading at northern Mid–Atlantic ridge

13/2018 Gandelli, E.; Penati, M.;Quaglini, V.;Lomiento, G.; Miglio, E.; Benzoni, G.M.
A novel OpenSees element for single curved surface sliding isolators